

Controlling Swarms of Bandit Inspector Spacecraft

Jeremy S. Neubauer

Graduate Student, Washington University in St. Louis

Michael A. Swartwout

Advisor, Washington University in St. Louis

The vast foreseeable benefits of on-orbit servicing to current and future space systems have sparked the development of both large-scale servicing spacecraft and small-scale technology demonstration platforms. The latter provide the ability to prove certain crucial technologies more efficiently than their larger counterparts, due to increased responsiveness and reduced cost. Washington University's Bandit is one such vehicle currently in progress, designed to research the sensory, autonomy, and control problems of the multi-vehicle, close-proximity flight necessary to nearly all of the on-orbit servicing industry's ambitions.

This study assesses the ability of behavior-based methods to solve the multi-Bandit control problem, complicated by the vehicle's highly constrained actuation, computation, and state observation capabilities. Herein, a potential function control system is tailored specifically for vehicles operating under such constraints. A stability analysis is derived that proves this controller will lead each inspector to its final desired equilibrium state within a calculable error bound, while multiple simulations of the system are used to validate this analysis and investigate its dynamic characteristics. Results indicate that the designed controller provides desirable performance in deployment, rendezvous, and station-keeping scenarios, and also shows promise in adapting to other servicing tasks, such as autonomous docking.

Introduction

Extending the operational lifetime and reliability of space systems requires many new on-orbit capabilities, including the ability to refuel, upgrade hardware, and detect and repair problems. Several research programs are aggressively pursuing these technologies, including NASA's DART, AFRL's XSS-10 and -11, NRL's SUMO, and DARPA's Orbital Express, to name a few. These vehicles, breaching 700 kg in size and \$100 million in price, plan to demonstrate all of these

abilities and more, and have already achieved some success^{1,2,3,4,5}.

The high cost and complexity of each of these missions is certainly necessary to accomplish such far reaching goals in a single flight. However, smaller scale projects can more responsively and efficiently test and prove subsets of these technologies. For instance, in June of 2000, Surrey Satellite Technology's 6.5 kg SNAP-1 demonstrated propulsion, 3-axis attitude stabilization, and target imaging capabilities with a relatively small investment of resources. Around the same time, both the Space Systems Laboratory at MIT and the Aerospace Systems Laboratory at Washington University in St. Louis began development of small satellite test beds for future on-orbit servicing technology demonstrations^{6,7}.

Washington University's Bandit is a free-flying, camera-carrying, nano-scale inspector spacecraft. On-board hardware is kept to a minimum by relegating long-period functions (power generation and long range communications) to a host vehicle, making the re-dockable drone small, agile, and inexpensive. Its diminutive stature maximizes compatibility with both host and launch vehicles, while minimizing assembly and integration times. Thus, low cost Bandit missions can be initiated quickly with nearly any host and launch vehicle, making the platform an extremely responsive test bed for developing on-orbit servicing technologies.

Close proximity flight of one or more service vehicles is perhaps the most crucial technology to the success of the industry, as it is a necessary stepping stone to all envisioned servicing operations. Accordingly, this study addresses the control problem of maneuvering multiple Bandit vehicles about a host. Beyond the universal guidance and collision avoidance issues, this matter is further complicated by Bandit's limited observational, computational, and actuation abilities. Due to the resultant need for simplicity and insensitivity to disturbances and dynamic

environments, it is hypothesized that behavior-based methods may be well suited to the task. After introducing the Bandit platform, this paper will proceed to review basic behavior-based control theory and its past applications to satellite control. Next, a controller designed specifically for Bandit swarms is proposed and assessed analytically. Finally, multiple simulations of on-orbit operations are conducted and examined.

The Bandit Platform

Bandit is a proposed research platform for on-orbit servicing technologies, specifically addressing the sensory, autonomy, and control problems of multi-vehicle, close-proximity operations. The first flight demonstration, currently under development via the University Nanosat-4 design competition, incorporates a 25kg Akoya host vehicle and two sub 5-kg deployable and re-dockable Bandit free-flyers. The mission seeks to demonstrate basic navigation and control abilities, proceeding from human piloted operations to limited autonomous maneuvers.

Each Bandit drone carries an eight thruster cold-gas propulsion system, with an integrated propellant tank capable of providing at least 12 m/s total ΔV . The thruster configuration was designed to provide decoupled translation and rotation about any single axis from a minimal number of jets, motivated by the size and cost of the requisite valves. Navigation is handled by a combination of three orthogonal MEMS rate gyros and a CMOS camera. Instrumenting the exterior of the host and each inspector with color-coded LEDs allows a Xilinx-based FPGA to convert images provided by the camera into relative position and attitude data at speeds up to 30 frames per second. An Atmel-based microcontroller manages command and data handling, also providing a 418 MHz, 4800 baud wireless short range (2 km) data link with Akoya. NiCad batteries supply the drones with up to 30 minutes of electrical power, including active heating for the propulsion and imaging systems.

The 45 cm tall, hexagonal Akoya host contains a similar vision system and battery pack, in addition to a 25 W solar cell power generation system, magnetically stabilized attitude control system, 5 W, 9600 baud telemetry downlink, and an array of Atmel-based microcontrollers. The distributed nature of the command & data handling system allows for the seamless addition or removal of entire subsystems – including Bandit drones. This feature provides a simple means of passing data and commands between the host and drones, as well as increased flexibility to

vary the total number of drones in the system. MEPSI based launch containers are included to physically accommodate the drones (Fig. 1), modified to allow for re-docking and recharging in flight. The device includes a motorized bay door to completely enclose the inspectors during launch, and an elevator platform to bring each drone to the surface for deployment.

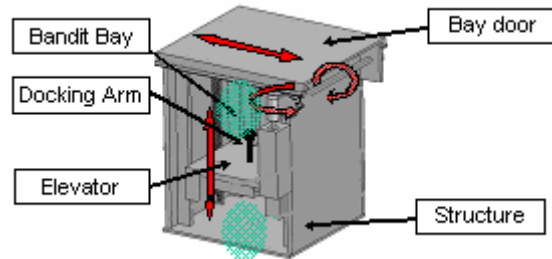


Fig. 1 Launch Container and On-Orbit Soft Dock

A metallic hook-and-loop system serves as the on-orbit “soft dock” (Fig. 2), while also providing a conductive path for recharging. The 2 cm hemispherical, hook covered pushrod tip on the elevator platform and loop covered Bandit exterior gives a large margin in docking angle and offset – up to 75° and 3 cm.



Fig. 2 Demonstration Soft Dock

To test the performance of the above hardware prior to flight, a three degree of freedom air bearing test bed has been developed (Fig. 3). To date, this system has been employed to show successful remotely-piloted proximity maneuvering (within 3 m) and soft docking, with relative closing velocities ranging from 0.5 to 100 cm/s. In addition, a Java-based, integrated operator workstation is under development to design and test various Bandit control algorithms – from human piloted versions to completely autonomous ones. Built upon a six degree of freedom simulator including the

effects of orbital dynamics and local disturbances, the remotely accessible program accurately reproduces the available telemetry data and reconstructs virtual images of the orbital scene (Fig. 4).

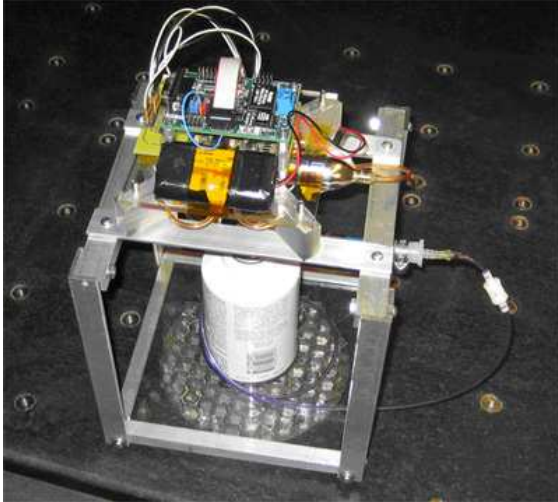


Fig. 3 Bandit and Air Bearing Testbed

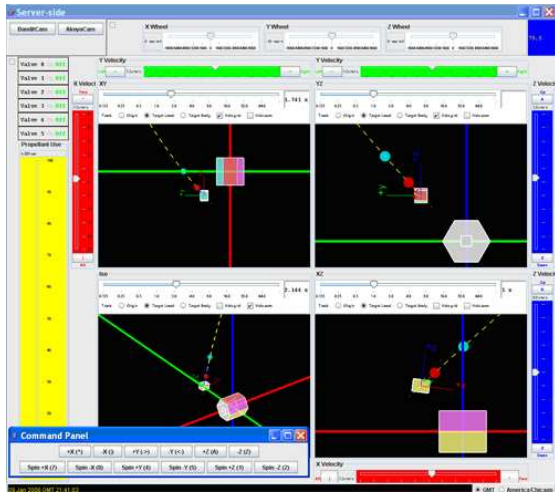


Fig. 4 GUI for Integrated Operator Workstation

Behavior-Based Control

Future Bandit missions will require the autonomous operation of multiple drones about a passive host – for example, the inspection of a foreign vehicle or object. The absence of an active supervisory host and the need for robustness to individual system failures dictates that each drone must operate in a completely decentralized fashion. These objectives, coupled with Bandit’s hardware constraints, make for a challenging control problem. Decentralization and minimal hardware limits the available state information to absolute

rotation rate and relative position, velocity, and orientation, while the image processing necessary to attain this data consumes the majority of the available computational resources, leaving little processing power to efficiently manage the eight thrusters that tightly restrict the available actuation space and couple translation to rotation. Therefore, a simple yet robust control algorithm is needed, which may be found within the theory of behavior-based methods.

Background

Behavior-based control methods work on the principle that complex global team behaviors can arise from simple individual vehicle behaviors, as seen in many biological systems. In fact, a prominent behavior-based control strategy in the literature follows the form of foraging tactics of the *E. coli* bacteria. It has been proposed that these bacteria, seeking to maximize their energy intake over time, effectively calculate a potential function based on the local distribution of food, toxins, and neighboring bacteria, then descend this potential to reach the most hospitable environment^{8,9}.

The application of such potential functions (also called gradient functions and artificial or structural potentials) to the control of autonomous vehicle teams has found much success. Several researchers have used the method to directly control vehicular velocity, while others directly control acceleration. In either case, the control action is calculated to maximize the rate of descent of the potential function. The resultant trajectories seek the potential function’s minimum value, which correlates to the preferred equilibrium state of the system^{10,11,12,13}.

The potentials are most often defined by inter-vehicle distances and are homogeneous across all vehicles, leading to uniformly triangulated geometric formations. In the genre of artificial physics, potential functions are based on the relative position and “spin” of the neighboring vehicles, thus creating more complex emergent spatial structures. The method’s similarity to the mechanics of atoms has resulted in behaviors akin to those seen in crystalline structures, including dislocations and phase-transitions^{14,15,16}.

A few researchers have applied potential-based methods to the control of satellites. McInnes has examined the matter on several occasions, studying impulsive rendezvous in the presence of obstacles, as well as large angle slew maneuvers, terminal descent guidance, and formation flight with continuous actuators^{17,18}. Ren and Beard have also investigated a

similar virtual structure technique applied to the formation flying problem, developing a decentralized controller that maintains accurate relative positioning of spacecraft using low-bandwidth communications¹⁹.

All of these behavior-based approaches have yielded similar results in gradient descent and formation dynamics, showing that complex system behaviors can in fact evolve from simple individual control laws. Yet it is important to note that detrimental group behaviors can be just as likely to occur as beneficial ones, highlighting the largest shortcoming of behavioral based control methods—few tools exist to analytically assess the stability and transient performance of the overall system. As a result, tuning parameters of complex potential function controllers typically mandates a trial and error approach, and can be quite time consuming. But they can offer several advantages in robustness to uncertain environments and vehicle failures (they are not model-based), tolerance of bandwidth limitations (they can perform without information of the total system state), and simplicity of implementation (they intrinsically have simple control laws at the individual level, requiring little processor power). Thus, they appear well suited to Bandit vehicle systems.

Bandit Applications

The simplicity and robustness of potential function methods make them good candidates for a Bandit control system. Yet the application of current potential function approaches to Bandit presents several problems, primarily due to Bandit's highly constrained actuator. Published methods for calculating a control and proving stability consistently assume a continuous time actuator, unconstrained in both direction and magnitude, whereas Bandit's thruster system is best considered discrete in time, and is highly limited in both the direction and magnitude of its control actions. Therefore a specialized controller must be designed, accounting for the specific needs and constraints of the Bandit spacecraft.

The controller developed in this study shares two key points with the published potential function methods of behavior-based control theory: (1) each vehicle computes potential functions based on the current state of the system, and (2) each vehicle seeks the minimum value of these potential functions. The details of the control logic therein differ substantially. Most notably, potential functions are defined by a velocity error rather than a position error, and the jet selection process is integrated with the guidance algorithm.

Control Logic

Much like the methods in the literature, each vehicle calculates its own Lyapunov function, defined simply as the sum of all pertinent potential functions. For this study, potentials for attitude (P_ω), position relative to the host (P_H), and position relative to other inspectors (P_I) are included, as in Eq. (1).

$$\Phi = P_\omega + P_H + P_I \quad (1)$$

Each of these potentials is driven by a velocity error. A typical formulation is that of Eq. (2), where \mathbf{v} is the current vehicular velocity, and \mathbf{v}_d is a desired velocity vector based on the state of the system, designed to lead the vehicle to its preferred equilibrium state.

$$P = k(\mathbf{v} - \mathbf{v}_d)^T (\mathbf{v} - \mathbf{v}_d) \quad (2)$$

The principle objective of the controller is to reduce Φ , thereby reducing velocity error. This format is chosen to complement the impulsive nature of Bandit's actuators, where control actions are defined by the instantaneous changes in translational and rotational velocity ($\Delta\mathbf{v}$ and $\Delta\boldsymbol{\omega}$) from the firing of a single jet for its minimum pulse width. Thus, control decisions can be made upon the instantaneous change of the Lyapunov function due to an impulse (Eq. (3)) and the cost of that impulse (σ) at each time step. The jet to fire is defined as that which satisfies and minimizes the triggering function of Eq. (4). If no thruster can satisfy this relation, no control action is taken.

$$\Delta\Phi = \Phi(\mathbf{v} + \Delta\mathbf{v}, \boldsymbol{\omega} + \Delta\boldsymbol{\omega}) - \Phi(\mathbf{v}, \boldsymbol{\omega}) \quad (3)$$

$$\Delta\Phi + \sigma \leq 0 \quad (4)$$

In the case of an unconstrained actuator, calculating a control as above is no easy task – given multiple nonlinear potentials, finding the optimal control impulse requires an iterative solution. Fortunately, the Bandit vehicle is constrained to as few as eight impulse options, entailing that as few as eight evaluations of the triggering function are necessary to select the best available jet.

Stability

The stability proof for this controller has two main parts. First, convergence to \mathbf{v}_d within a defined error bound is shown. Then, convergence to the equilibrium position is shown, taking into account said error bound on velocity.

For this proof, a general Lyapunov function of the form of Eq. (5) is considered, where translational velocity errors are indicated by $\mathbf{v}_{e,i}$, rotational velocity errors are indicated by $\boldsymbol{\omega}_{e,j}$, and $k_{v,i}$ and $k_{\omega,j}$ are all strictly positive. The change in Φ from an impulse is then given by Eq. (6).

$$\Phi = \sum_i k_{v,i} \mathbf{v}_{e,i}^T \mathbf{v}_{e,i} + \sum_j k_{\omega,j} \boldsymbol{\omega}_{e,j}^T \boldsymbol{\omega}_{e,j} \quad (5)$$

$$\begin{aligned} \Delta\Phi &= \sum_i k_{v,i} \left(2\mathbf{v}_{e,i}^T \Delta\mathbf{v} + |\Delta\mathbf{v}|^2 \right) \\ &+ \sum_j k_{\omega,j} \left(2\boldsymbol{\omega}_{e,j}^T \Delta\boldsymbol{\omega} + |\Delta\boldsymbol{\omega}|^2 \right) \end{aligned} \quad (6)$$

Combining Eqs. (4) and (6) provides a detailed look at the necessary criteria for firing a thruster (Eq. (7)).

$$\begin{aligned} &2 \left[\sum_i k_{v,i} \mathbf{v}_{e,i}^T \quad \sum_j k_{\omega,j} \boldsymbol{\omega}_{e,j}^T \right] \begin{bmatrix} \Delta\mathbf{v} \\ \Delta\boldsymbol{\omega} \end{bmatrix} \\ &+ \sum_i k_{v,i} |\Delta\mathbf{v}|^2 + \sum_j k_{\omega,j} |\Delta\boldsymbol{\omega}|^2 + \sigma \leq 0 \end{aligned} \quad (7)$$

When this statement is true, a thruster is fired that decreases Φ , entailing the decrease of $\left| \sum_i k_{v,i} \mathbf{v}_{e,i}^T \quad \sum_j k_{\omega,j} \boldsymbol{\omega}_{e,j}^T \right|$ and convergence to the desired velocities. Recognizing that the σ , $|\Delta\mathbf{v}|$, and $|\Delta\boldsymbol{\omega}|$ terms are each greater than zero for all system states, only two cases exist for which a thruster will not be fired. First, it could be that a control action is not available to make $\left[\sum_i k_{v,i} \mathbf{v}_{e,i}^T \quad \sum_j k_{\omega,j} \boldsymbol{\omega}_{e,j}^T \right] \begin{bmatrix} \Delta\mathbf{v} \\ \Delta\boldsymbol{\omega} \end{bmatrix} < 0$, implying that some combinations of velocity errors (no matter their magnitude) are not correctable. This scenario must be avoided by the proper design of the thruster

configuration, a condition described mathematically in Eq. (8), where $\begin{bmatrix} \Delta\mathbf{v} \\ \Delta\boldsymbol{\omega} \end{bmatrix}_k$ is the effect of firing thruster k .

$$\forall \mathbf{x}_{1 \times 6} \exists \begin{bmatrix} \Delta\mathbf{v} \\ \Delta\boldsymbol{\omega} \end{bmatrix}_k : \mathbf{x} \begin{bmatrix} \Delta\mathbf{v} \\ \Delta\boldsymbol{\omega} \end{bmatrix}_k < 0 \quad (8)$$

Meeting this requirement entails that the union of open half spaces defined by the $\begin{bmatrix} \Delta\mathbf{v} \\ \Delta\boldsymbol{\omega} \end{bmatrix}_k$ vectors occupies the entire six dimensional space (excluding the origin). This property is herein denoted as complete control authority.

Given a vehicle with this property, the only remaining case for which a thruster may not be fired is when all velocity errors are small, and, although the first term of Eq. (7) can be made negative, it can not completely counteract the later positive terms. This implies that there exists a set of small magnitude velocity errors that cannot be corrected. This space, driven by σ and the size of the minimum thrust bit, can be identified by first calculating an upper bound to the first term of Eq. (7) as stated in Eq. (9). α is a positive constant determined by the specific configuration of the vehicle's thrusters.

$$\begin{aligned} &2 \left[\sum_i k_{v,i} \mathbf{v}_{e,i}^T \quad \sum_j k_{\omega,j} \boldsymbol{\omega}_{e,j}^T \right] \begin{bmatrix} \Delta\mathbf{v} \\ \Delta\boldsymbol{\omega} \end{bmatrix} \\ &\leq -\alpha \left| \sum_i k_{v,i} \mathbf{v}_{e,i}^T \quad \sum_j k_{\omega,j} \boldsymbol{\omega}_{e,j}^T \right| \end{aligned} \quad (9)$$

Combining this upper bound with the triggering function yields a revised criteria for thruster activation based on the state in Eq. (10).

$$\begin{aligned} &\frac{\sum_i k_{v,i} |\Delta\mathbf{v}|^2 + \sum_j k_{\omega,j} |\Delta\boldsymbol{\omega}|^2 + \sigma}{\alpha} \\ &\leq \left| \sum_i k_{v,i} \mathbf{v}_{e,i}^T \quad \sum_j k_{\omega,j} \boldsymbol{\omega}_{e,j}^T \right| \end{aligned} \quad (10)$$

The maximum composite error bound is defined by the largest error that can exist without triggering a corrective thruster to fire, and is thus given by the equality of Eq. (10). Individual error bounds can be calculated by considering each potential independently, setting all other potentials to zero, resulting in the allowable error Eqs. (11) and (12). Beyond these error bounds, a thruster that reduces total velocity error

will be found and fired; therefore, the vehicle must converge to a velocity near the desired velocity within the bounds of Eqs. (11) and (12).

$$|\mathbf{v}_{e,i}| < \frac{\sum_i k_{v,i} |\Delta \mathbf{v}|^2 + \sum_j k_{\omega,j} |\Delta \boldsymbol{\omega}|^2 + \sigma}{\alpha k_{v,i}} \quad \forall i \quad (11)$$

$$|\boldsymbol{\omega}_{e,j}| < \frac{\sum_i k_{v,i} |\Delta \mathbf{v}|^2 + \sum_j k_{\omega,j} |\Delta \boldsymbol{\omega}|^2 + \sigma}{\alpha k_{\omega,j}} \quad \forall j \quad (12)$$

To ensure velocity remains within these bounds once they have been reached, the time rate of change of \mathbf{v}_d and $\boldsymbol{\omega}_d$ must be less than the acceleration abilities of the craft, as stated in Eqs. (13) and (14).

$$T_s \frac{d}{dt} (\mathbf{v}_d) < \Delta \mathbf{v} \quad (13)$$

$$T_s \frac{d}{dt} (\boldsymbol{\omega}_d) < \Delta \boldsymbol{\omega} \quad (14)$$

The investigation of position convergence begins under the assumption that the vehicle has attained a velocity near that desired as described above. For the vehicle to be heading towards the desired position, its instantaneous velocity vector must be oriented such that position error is reducing. For the translational case where only one potential commands convergence to \mathbf{r}_d , this criteria is defined by Eq. (15).

$$(\mathbf{v}_{d,1} + \mathbf{v}_{e,1})^T (\mathbf{r}_d - \mathbf{r}) > 0 \quad (15)$$

Clearly, the worst case for position convergence is when the velocity error is directed opposite the position error, $\mathbf{r}_e = \mathbf{r}_d - \mathbf{r}$, and of the maximum allowable magnitude defined by Eq. (11). Applying this case to the above equation yields Eq. (16)

$$\mathbf{v}_{d,1}^T \mathbf{r}_e > \frac{\sum_i k_{v,i} |\Delta \mathbf{v}|^2 + \sum_j k_{\omega,j} |\Delta \boldsymbol{\omega}|^2 + \sigma}{\alpha k_{v,1}} |\mathbf{r}_e| \quad (16)$$

With knowledge of $\mathbf{v}_{d,1}$, Eq. (16) can be employed to calculate a convergence envelope. For the velocity

field of Eq. (17), where $f(\mathbf{r}_e) \geq 0$, that envelope is defined by Eq. (18).

$$\mathbf{v}_d = f(\mathbf{r}_e) \frac{\mathbf{r}_e}{|\mathbf{r}_e|} \quad (17)$$

$$f(\mathbf{r}_e) > \frac{\sum_i k_{v,i} |\Delta \mathbf{v}|^2 + \sum_j k_{\omega,j} |\Delta \boldsymbol{\omega}|^2 + \sigma}{\alpha k_{v,1}} \quad (18)$$

As it is expected that $f(\mathbf{r}_e)$ will increase with $|\mathbf{r}_e|$, the convergence envelope will encompass the entire state space excluding a small area near \mathbf{r}_d . However, it is possible to create an empty convergence space via poor design of the thruster configuration and control parameters.

The rotational position convergence argument follows similar logic. First, it is assumed that only one potential directs convergence to the desired orientation, creating the convergence condition defined in Eq. (19). Here, the desired orientation is defined by the alignment of the inspector's camera look vector, $\hat{\mathbf{n}}$, and the normalized relative position vector of its target, $\hat{\mathbf{r}}$.

$$(\boldsymbol{\omega}_{d,1} + \boldsymbol{\omega}_{e,1})^T \left(\frac{\hat{\mathbf{n}} \times \hat{\mathbf{r}}}{|\hat{\mathbf{n}} \times \hat{\mathbf{r}}|} \right) > 0 \quad (19)$$

Applying the same worst case condition as before leads to the new relation of Eq. (20):

$$\boldsymbol{\omega}_{d,1}^T \left(\frac{\hat{\mathbf{n}} \times \hat{\mathbf{r}}}{|\hat{\mathbf{n}} \times \hat{\mathbf{r}}|} \right) > \frac{\sum_i k_{v,i} |\Delta \mathbf{v}|^2 + \sum_j k_{\omega,j} |\Delta \boldsymbol{\omega}|^2 + \sigma}{\alpha k_{\omega,j}} \quad (20)$$

The convergence envelope can now be calculated with knowledge of $\boldsymbol{\omega}_d$. For $\boldsymbol{\omega}_d$ as defined in Eq. (21), where $g(\hat{\mathbf{n}}, \hat{\mathbf{r}})$ is strictly positive, Eq. (22) defines that envelope. Again assuming a $g(\hat{\mathbf{n}}, \hat{\mathbf{r}})$ that increases with increasing orientation error, the convergence space only excludes a small region around the desired orientation.

$$\boldsymbol{\omega}_d = g(\hat{\mathbf{n}}, \hat{\mathbf{r}}) \left(\frac{\hat{\mathbf{n}} \times \hat{\mathbf{r}}}{|\hat{\mathbf{n}} \times \hat{\mathbf{r}}|} \right) \quad (21)$$

$$g(\hat{\mathbf{n}}, \hat{\mathbf{r}}) > \frac{\sum_i k_{v,i} |\Delta \mathbf{v}|^2 + \sum_j k_{\omega,j} |\Delta \boldsymbol{\omega}|^2 + \sigma}{\alpha k_{\omega,j}} \quad (22)$$

At this point, convergence to a bounded area around the desired equilibrium state has been shown for a single vehicle. For the case of a single vehicle with only one rotational and one translational potential, some quantification of the transient behavior of the system can be made through knowledge of the desired velocities, maximum velocity error bounds (Eqs. (11) and (12)), and initial conditions. For the case of multiple vehicles, potentials, and disturbances, however, little can be said of the path taken to equilibrium. Unfortunately, this case is of particular interest, as the possibility of collision exists. In this study, collision avoidance will be addressed solely through simulation.

Rotational Potential

The desired rotational response for the Bandit spacecraft is to continually point its camera at a predefined target. Attempting to meet this goal via a quaternion error vector or similar approach over constrains the problem by enforcing a particular attitude about the camera's look vector. Accordingly, a simplified approach is taken to align the camera look vector with the host's normalized relative position vector. For the standard form potential in Eq. (23), the desired angular velocity of Eq. (24) will yield this desired response.

$$P_{\omega} = k_{\omega} (\boldsymbol{\omega} - \boldsymbol{\omega}_d)^T (\boldsymbol{\omega} - \boldsymbol{\omega}_d) \quad (23)$$

$$\boldsymbol{\omega}_d = \left(\mu_{\omega} \sqrt{1 - \hat{\mathbf{n}} \cdot \hat{\mathbf{r}}} \right) \frac{\hat{\mathbf{n}} \times \hat{\mathbf{r}}}{|\hat{\mathbf{n}} \times \hat{\mathbf{r}}|} \quad (24)$$

The cross product terms in $\boldsymbol{\omega}_d$ provide its direction, while the remaining term, $(\mu_{\omega} \sqrt{1 - \hat{\mathbf{n}} \cdot \hat{\mathbf{r}}})$, provides its magnitude. A plot of $\boldsymbol{\omega}_d$ for a single rotational degree of freedom case is illustrated below in Fig. 5, where $\theta_e = \cos^{-1} \hat{\mathbf{n}} \cdot \hat{\mathbf{r}}$. Note that the desired velocity is always towards the alignment of $\hat{\mathbf{n}}$ and $\hat{\mathbf{r}}$, increasing in magnitude with increasing distance from equilibrium.

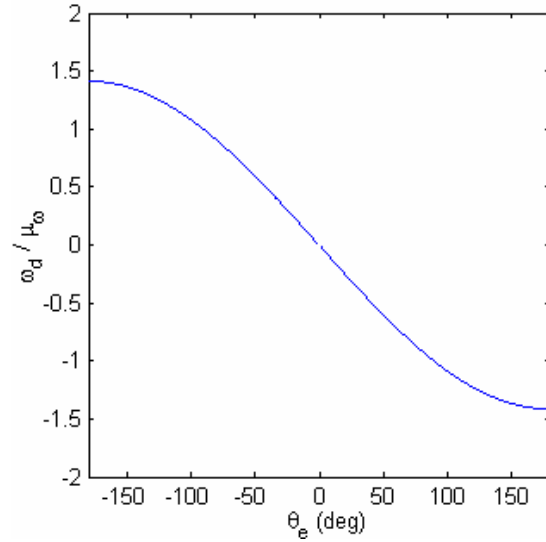


Fig. 5 Desired Angular Velocity

Host Potential

To achieve and maintain the desired imaging distance, a host potential is employed based on the standard form potential of Eq. (25). The included velocity error, Eq. (26), is defined as a function of a position error vector, Eq. (27), where r_d is the desired imaging distance between the target and inspector.

$$P_H = k_H (\mathbf{v} - \mathbf{v}_d)^T (\mathbf{v} - \mathbf{v}_d) \quad (25)$$

$$\mathbf{v}_d = \frac{\mu_H}{1 + |\mathbf{r}_e|} \mathbf{r}_e \quad (26)$$

$$\mathbf{r}_e = \left(1 - \frac{r_d}{|\mathbf{r}|} \right) \mathbf{r} \quad (27)$$

The form of Eqs. (26) and (27) were selected to yield a linearly increasing \mathbf{v}_d around $\mathbf{r}_e = 0$ with a limited maximum value of μ_H as $\mathbf{r}_e \rightarrow \infty$. A plot of \mathbf{v}_d versus \mathbf{r}_e in Fig. 6 illustrates these traits below.

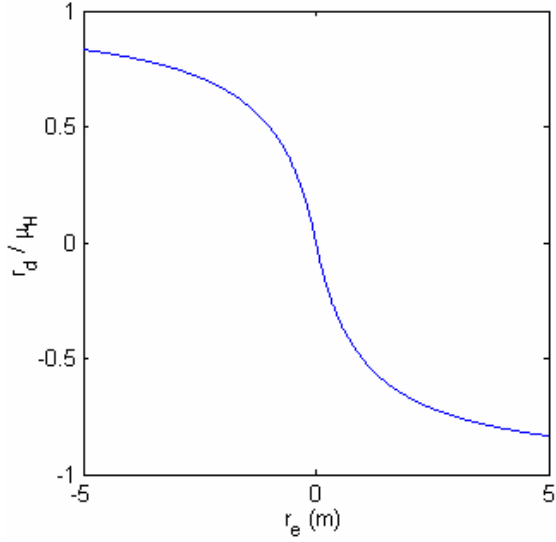


Fig. 6 Desired Translational Velocity

Inter-Vehicle Potential

Applying this method to control inter-vehicle spacing is not as straightforward as the two previous cases. At close distances, where the chance of collision is high, it is desired that the vehicles generate velocities away from one another; but at larger distances, no specific relation between vehicle velocities is necessary. To capture these needs, a potential of the form of Eq. (28) is employed. Here, \mathbf{r}_{lm} and \mathbf{v}_{lm} are the position and velocity vectors of vehicle l relative to vehicle m .

$$P_{l,l} = \sum_m \frac{k_{l,m}}{|\mathbf{r}_{lm}|} (\mathbf{v}_{lm} - \mathbf{v}_{d,l,m})^T (\mathbf{v}_{lm} - \mathbf{v}_{d,l,m}) \quad (28)$$

The inclusion of the inter-vehicle spacing in the potential definition tells the controller when matching vehicle velocity to $\mathbf{v}_{d,l,m}$ is beneficial. When inter-vehicle distances are large, the effect of a change in inter-vehicle velocities on the total Lyapunov function is null. However, when inter-vehicle distances are small, the effect of such changes on Φ are amplified. The desired inter-vehicle velocity used in this study is simply a constant magnitude velocity directed away from the neighboring vehicle, as defined in Eq. (29).

$$\mathbf{v}_{d,l,m} = \frac{\mu_{l,l}}{|\mathbf{r}_{lm}|} \mathbf{r}_{lm} \quad (29)$$

Parameter Selection

Given a vehicle with a predetermined thruster system (defining α and each $\begin{bmatrix} \Delta \mathbf{v} \\ \Delta \boldsymbol{\omega} \end{bmatrix}_k$), eight parameters are available to tune system response: r_d , μ_H , μ_ω , μ_I , k_H , k_ω , k_I , and σ . The first four can be set directly from mission requirements – r_d is determined by the onboard camera and necessary imaging quality, while μ_H , μ_ω , and μ_I , are determined from the maximum desired vehicle velocities. Maximum bounds on μ_H and μ_ω are provided by the need to maintain velocity convergence, as noted in Eqs. (13) and (14). Combining these relations with \mathbf{v}_d and $\boldsymbol{\omega}_d$ as described earlier provides Eqs. (30) and (31):

$$\mu_H < \sqrt{\frac{\Delta \mathbf{v}}{T_s}} \quad (30)$$

$$\mu_\omega < \sqrt{\frac{2\Delta \boldsymbol{\omega}}{T_s}} \quad (31)$$

This leaves the three potential gains and the cost function to be selected by the control system designer. Noting that the absolute values of these four parameters is inconsequential, one gain (k_H) can be set to unity. Next, the desired steady state response and convergence envelope equations can be employed to calculate k_ω and σ . Using the specific potentials described by Eqs. (23) to (29), and assuming sufficient inter-vehicle spacing and velocity to ignore P_I , Eqs. (32) and (33) determine the maximum steady state errors $\theta_{e,ss}$ and $r_{e,ss}$. Then, given desired $\theta_{e,ss}$ and $r_{e,ss}$ values, these equations can be solved simultaneously to find k_ω and σ .

$$\theta_{e,ss} = \cos^{-1} \left(1 - \left[\frac{|\Delta \mathbf{v}|^2 + k_\omega |\Delta \boldsymbol{\omega}|^2 + \sigma}{\alpha k_\omega \mu_\omega} \right]^2 \right) \quad (32)$$

$$r_{e,ss} = \frac{|\Delta \mathbf{v}|^2 + k_\omega |\Delta \boldsymbol{\omega}|^2 + \sigma}{\alpha \mu_H - |\Delta \mathbf{v}|^2 - k_\omega |\Delta \boldsymbol{\omega}|^2 - \sigma} \quad (33)$$

The sole remaining parameter, k_I , remains to be determined by iterative simulation.

Simulation Results

A six degree of freedom simulation incorporating relative Clohessy-Wiltshire orbit dynamics was constructed in Matlab to assess the expected performance of the above controller. The code was designed to allow for user definable thruster configurations, potential functions, number of vehicles, and orbit environments. For the following results, a team of six hypothetical Bandit vehicles with the properties of Table 1 and Fig. 7 was examined in a circular 275 km altitude orbit.

Using a nonlinear search algorithm, this thruster configuration yielded $\alpha = 2.04\text{e-}4$, corresponding to best possible steady state error bounds of $r_{e,ss} \leq 6.2$ mm and $\theta_{e,ss} \leq 67$ degrees. The large discrepancy between translational and rotational accuracy is due to the wide variation in scale between $\Delta\mathbf{v}$ (0.25 mm/s) and $\Delta\boldsymbol{\omega}$ (4.0 mrad/s). In cases such as these, it is best to consider rotation and translation separately for the purposes of computing a convergence envelope and selecting control parameters. Doing so reveals $\alpha_v = 2.88\text{e-}4$ and $\alpha_\omega = 2.20\text{e-}3$, corresponding to best possible steady state error bounds of $r_{e,ss} \leq 4.4$ mm and $\theta_{e,ss} \leq 5.9$ degrees.

The desired imaging distance was selected as $r_d = 5$ m, with desired max steady state errors of $r_{e,ss} = 0.5$ m and $\theta_{e,ss} = 10$ deg. Desired velocities of $\mu_H = 5$ cm/s, $\mu_\omega = 0.1$ rad/s, and $\mu_v = 5$ cm/s were also selected. Applying a nonlinear search algorithm to solve Eqs. (32) and (33) for these values gives $k_\omega = 0.177$ and $\sigma = 1.90\text{e-}6$. After a few simulations, the inter-vehicle potential gain was chosen as $k_I = 0.100$.

Two simulation cases are presented. In the first case, the six Bandit vehicles were clustered closely together 0.5 meters away from the host, indicative of an initial deployment scenario. In the second case, the vehicles were again clustered together, but at a distance of roughly 17 meters from the host. This scenario is representative of a short range rendezvous that would be necessary to inspect a foreign target. For each case, the initial translational velocities were zero, while the spin rates varied in direction with a total magnitude of approximately 0.1 rad/s per vehicle.

Attitude data for vehicle one of the rendezvous simulation is examined in Fig. 8. Note the quick initial despin and convergence to the desired orientation, as well as the low magnitude steady state error oscillation. This data is extremely similar for all vehicles across both simulations, and thus is only presented once for brevity.

Table 1 Bandit Physical Properties

<i>Mass</i>	2 kg
<i>X, Y, & Z Mass Moment of Inertia</i>	7.5 g*m ²
<i>Thrust Magnitude</i>	50 mN
<i>Sampling Period / Thrust Duration</i>	0.01 sec.
<i>Minimum $\Delta\mathbf{V}$</i>	0.25 mm/s

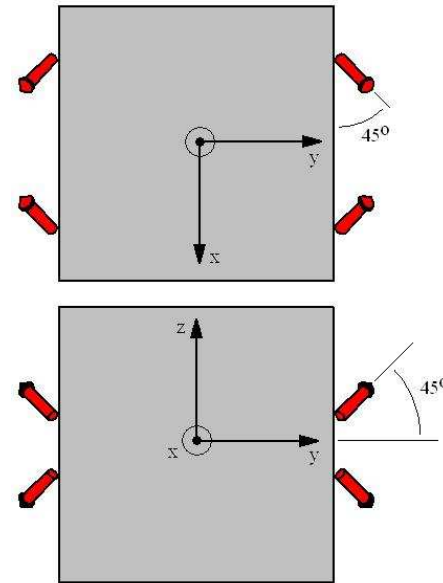


Fig. 7 Bandit Thruster Orientation

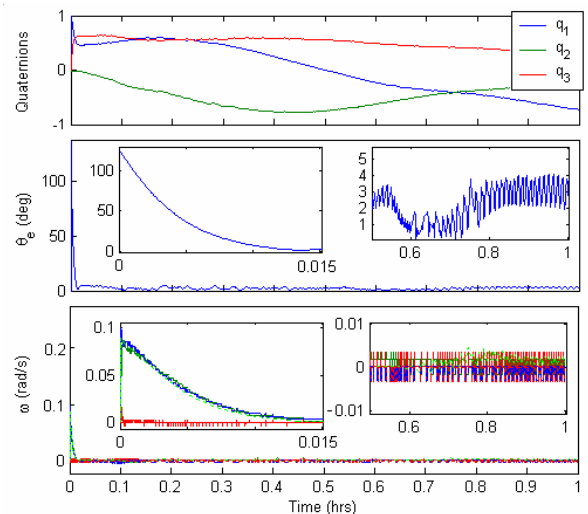


Fig. 8 Representative Attitude Response

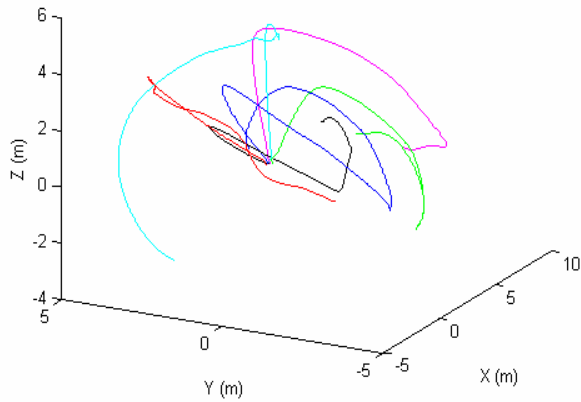


Fig. 9 Initial Deployment Trajectories

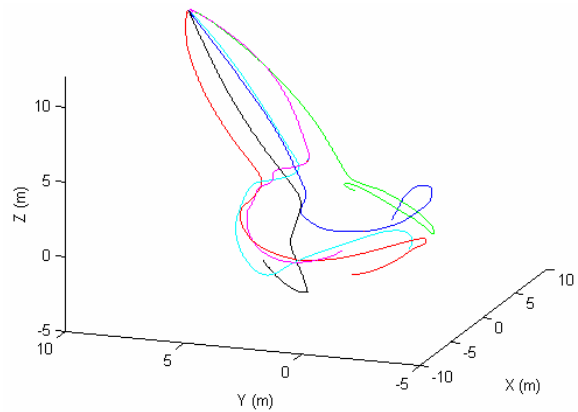


Fig. 11 Rendezvous Trajectories

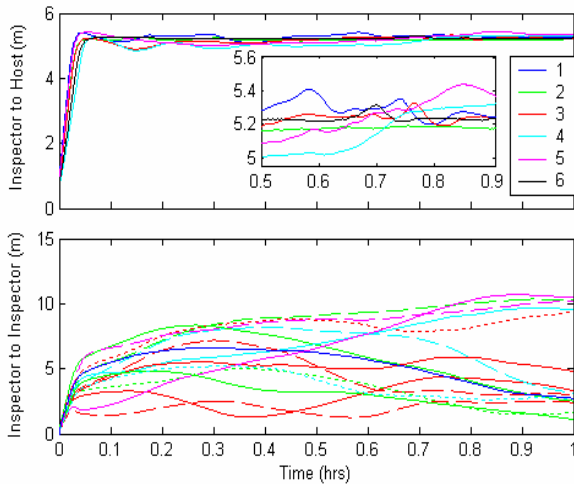


Fig. 10 Initial Deployment Relative Distances

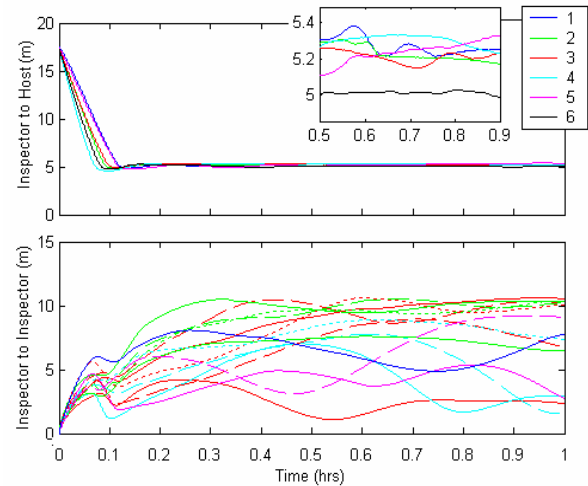


Fig. 12 Rendezvous Relative Distances

The trajectories of each vehicle in the Clohessy-Wiltshire coordinate frame (with the host positioned at the origin) are presented in Fig. 9 and Fig. 11 for both simulations. Relative distance histories are displayed in Fig. 10 and Fig. 12, including inspector to host and inspector to inspector data.

The first comment to be made about the above results is that the potentials direct the trajectories as desired, despite the relative orbit dynamics, constrained, impulsive actuators, and extremely limited state knowledge. With no communication and only relative position and velocity data, the Bandit vehicles converge to their desired positions and orientations without collision.

These simulations also show the validity of the derived analytical methods for selecting control gains and predicting convergence and steady state error bounds.

The k_ω and σ gains provided by Eqs. (32) and (33) produced desirable host-relative maneuvering without the need for iterative simulation, yielding convergence to the specified equilibrium state well within the predicted steady state error bounds.

Examining the propellant consumption data in Table 2 reveals that the majority of the fuel cost occurs within the first few seconds of flight. This is due to the quick removal of the initial spin rate and promptly accelerating to the desired translational velocity. Once this period is over, propellant consumption averages 0.1195 m/s per hour – providing a maximum total flight time of over 100 hours for the minimum Bandit fuel supply. Assuming a worst case consumption rate of 2.38 m/s per hour, total flight time drops to five hours. Recalling that Bandit is battery limited to 30 minutes of flight before re-docking, this translates to no less than ten individual sorties.

Table 2 Propellant Consumption Data

Simulation Case	Consumed Δv (m/s per hr)		
	Avg.	Min	Max
<i>Deployment, 0 to 1hr</i>	0.2823	0.2225	0.3588
<i>Deployment, 0 to 0.1 hrs</i>	1.7588	1.3754	2.2725
<i>Deployment, 0.1 to 1 hr</i>	0.1182	0.0944	0.1461
<i>Rendezvous, 0 to 1 hr</i>	0.3294	0.2850	0.4000
<i>Rendezvous, 0 to 0.15 hrs</i>	2.0850	1.6975	2.3775
<i>Rendezvous, 0.15 to 1 hr</i>	0.1209	0.0438	0.1705

Conclusions & Future Work

The methods developed in this study extend the limits of potential function control theory, specifically in its application to vehicles with constrained, impulsive actuators. A stability proof has been derived, as well as analytical approaches to calculating steady state error bounds and controller gains. These abilities greatly simplify the tuning process – which has long been a major stumbling block of potential function methods. Specific potentials for the Bandit vehicle were also developed to yield target pointing and collision avoidance based on limited sensory data. The complete controller provides immense simplicity of on-board implementation, as well as seamless scalability to large numbers of drones.

The two cases simulated for this study – deployment and short range rendezvous of six inspectors – verify the derived analytical methods and show desirable dynamic characteristics. State histories reveal short rise and settling times, as well as steady-state errors (5° and 0.5 m) within the analytical projections of the stability analysis. Sustained station keeping maneuvers averaged 0.1195 m/s of propellant consumption per hour, corresponding to a minimum lifetime of over 100 hours for the minimum Bandit fuel supply.

These results show that the potential function method developed herein is quite capable of controlling swarms of Bandit inspector spacecraft. As discussed above, dynamic characteristics have met or exceeded their targets, while propellant consumption has been kept to acceptable levels. Additionally, the robustness of its potential function core provides the ability to overcome expected in-flight disturbances, and its seamless scalability allows the operation of one or dozens of vehicles. As none of these abilities were

previously achievable within the craft’s limited observational, computational, and actuation abilities, this potential function controller is a key enabling technology for Bandit-class vehicles. Ergo, the Bandit system is now well positioned to provide a responsive test bed for researching on-orbit servicing technologies.

Future work will expand on the capabilities of this general control framework with regard to proximity flight and on-orbit servicing. First, alternative inter-vehicle potentials will be explored; specifically ones that account for the actual risk of a collision. Next, autonomous docking will be approached. The controller shows promise with respect to docking due to its ability to accurately track velocity commands; the only adaptation necessary is a specific docking velocity field. Fixing the field to the host vehicle could allow successful docking even in the presence of a tumble.

Another avenue to be pursued is the feedback of image quality into velocity commands. Properly incorporating this data into the host potential could allow Bandit to identify the optimal imaging distance independently – a skill necessary to inspecting foreign objects and adapting to changing environments. Additionally, by leveraging the short range communication abilities of the inspectors, repeated inspection of the same surface could be avoided, creating a more efficient surveillance process.

In parallel to further controller development, experimental testing on the ASL’s integrated operator workstation and air bearing test bed is planned. The workstation will be used to investigate robustness to model inaccuracies and thruster failures, as well as operation with an increased number of vehicles. Testing on the air bearing test bed will concern the integration of this controller with hardware and the navigation and image processing systems.

References

- ¹ http://www.space.com/spaceneews/militaryspace/DARUpdate_042205.html [cited 4-27-2005]
- ² Davis, Thomas M. et. al., "XSS-10 Micro-Satellite Flight Demonstration Program," *Proceedings of the 17th Annual AIAA/USU Conference on Small Satellites*, Logan, UT August 2003.
- ³ <http://www.vs.af.mil/Factsheets/XSS11-MicroSatellite.pdf> [cited 4-27-2005]
- ⁴ <http://www.darpa.mil/tto/programs/oe.htm>
- ⁵ Bosse, Albert B., et. al., "SUMO: Spacecraft for the Universal Modification of Orbits," *Defense and Security Symposium Proceedings*, Orlando, FL, April 2004.
- ⁶ Chen, Allen, et. al., "Development of Formation Flight and Docking Algorithms Using the Spheres Testbed," *Proceedings of the 15th Annual AIAA/USU Conference on Small Satellites*, Logan, UT, August 2001.
- ⁷ Swartwout, Michael, et. al., "The Bandit: An Automated Vision-Navigated Inspector Spacecraft," *Proceedings of the 17th Annual AIAA/USU Conference on Small Satellites*, Logan, UT, August 2003.
- ⁸ Passino, Kevin M., "Distributed Optimization and Control Using Only a Germ of Intelligence," Plenary Address, Third Congress of the Colombian Association for Automation, Rionegro, Colombia, South America, September 1998.
- ⁹ Liu, Y, and K.M. Passino, "Biomimicry of Social Foraging Behavior for Distributed Optimization: Models, Principles, and Emergent Behaviors," *Journal of Optimization Theory and Applications*, Vol. 115, No. 3, December 2002, pp. 603-628.
- ¹⁰ P. Ögren, E. Fiorelli and N. Leonard, "Formations with a mission: Stable coordination of vehicle group maneuvers," *15th Int. Symposium on Mathematical Theory of Networks and Systems*, Indiana, Aug. 2002.
- ¹¹ Olfati-Saber, R., and R. Murray. "Distributed cooperative control of multiple vehicle formations using structural potential functions," *Proceedings of the IFAC World Congress*, Barcelona, Spain. July 2002.
- ¹² Leonard, Naomi Ehrlich, and Edward Fiorelli, "Virtual leaders, Artificial Potentials and Coordinated Control of Groups," *Proceedings of the IEEE International Conference on Decision and Control*, Orlando, FL, December 2001.
- ¹³ Tanner, Herbert G., Ali Jadbabaie, and George J. Pappas, "Coordination of Multiple Autonomous Vehicles," *11th Mediterranean Conference on Control and Automation*, 2003.
- ¹⁴ Spears, William M., and Diana F. Gordon, "Using Artificial Physics to Control Agents," *IEEE International Conference on Information, Intelligence, and Systems*, November, 1999.
- ¹⁵ Gordon, Diana F., et al., "Distributed Spatial Control, Global Monitoring and Steering of Mobile Physical Agents," *IEEE International Conference on Information, Intelligence, and Systems*, November, 1999.
- ¹⁶ Gordon, Diana F., and William M. Spears, "Analysis of a Phase Transition in a Physics-Based Multiagent System," *Formal Approaches to Agent-Based Systems*, 2002.
- ¹⁷ Lopez, Ismael, and C.R. McInnes, "Autonomous Rendezvous Using Artificial Potential Function Guidance," *Journal of Guidance, Control, and Dynamics*, Vol. 18, No. 2, March-April 1995, pp. 237-241.
- ¹⁸ McInnes, C.R., "Potential Function Methods for Autonomous Spacecraft Guidance and Control," *AAS/AIAA Astrodynamics Specialist Conference*, Halifax, NS, Canada, August 1995.
- ¹⁹ Ren, W. and Randal W. Beard, "Formation Feedback Control for Multiple Spacecraft via Virtual Structures," *IEE Proceedings – Control Theory and Applications*, Vol. 151, No. 3, May 2004.